Elastin-Derived Peptides Are New Regulators of Insulin Resistance Development in Mice

Sébastien Blaise,[1] Béatrice Romier,[1] Charlotte Kawecki,[1] Maxime Ghirardi,[1] Fanja Rabenoelina,[1] Stéphanie Baud,[1] Laurent Duca,[1] Pascal Maurice,[1] Andrea Heinz,[2] Christian E.H. Schmelzer,[2] Michel Tarpin,[1] Laurent Martiny,[1] Christian Garbar,[3] Manuel Dauchez,[1] Laurent Debelle,[1] and Vincent Durlach[1,4]

Although it has long been established that the extracellular matrix acts as a mechanical support, its degradation products, which mainly accumulate during aging, have also been demonstrated to play an important role in cell physiology and the development of cardiovascular and metabolic diseases. In the current study, we show that elastin-derived peptides (EDPs) may be involved in the development of insulin resistance (IRES) in mice. In chow-fed mice, acute or chronic intravenous injections of EDPs induced hyperglycemic effects associated with glucose uptake reduction and IRES in skeletal muscle, liver, and adipose tissue. Based on in vivo, in vitro, and in silico approaches, we propose that this IRES is due to interaction between the insulin receptor (IR) and the neuraminidase-1 subunit of the elastin receptor complex triggered by EDPs. This interplay was correlated with decreased sialic acid levels on the β-chain of the IR and reduction of IR signaling. In conclusion, this is the first study to demonstrate that EDPs, which mainly accumulate with aging, may be involved in the insidious development of IRES. ***Diabetes*** **62:3807–3816, 2013**

The extracellular matrix (ECM) is one of the most important regulators of cellular and tissue function in the body. Tightly controlled, ECM homeostasis is essential for organ physiology. This is mirrored by the fact that the ECM is dysregulated in many different types of disease such as cardiovascular and metabolic diseases (1). The vascular matrix is mainly composed of collagen and elastin fibers (2). The nature of the elastin chains and its strong reticulation make elastin a highly stable molecule with longevity comparable to the human life span. Consequently, elastin essentially undergoes no turnover and is irreparable (3). During physiological and pathophysiological aging, such as inflammation or atherosclerosis, elastin is prone to proteolytic degradation (4,5). Indeed, increased elastase activity associated with increased lipids and calcium deposits leads to elastin fragmentation. Importantly, the generated peptides, also known as elastin-derived peptides (EDPs), are bioactive elements and can accentuate the progression of disease (1). A typical EDP is the VGVAPG hexapeptide, which has a sequence repeated in tandem six times in the human tropoelastin sequence. As in most bioactive EDPs, VGVAPG bears a GXXPG motif, allowing formation of a type VIII β-turn required for binding to its cognate receptor, the elastin receptor complex (ERC) (6). This widely expressed receptor complex comprises a peripheral EDP-binding subunit, the so-called elastin binding protein (EBP), a protective protein/cathepsin A, and neuraminidase-1 (Neu-1), whose enzymatic activity is required for ERC signaling (7). Neu-1 can cleave terminal *N*-glycosidic sialic acid in various sialoconjugates, ranging from glycoproteins to glycolipids. Interestingly, this enzyme has been proposed to be a modulator of various cell receptors (8).

Recently, insulin resistance (IRES) has been linked to expression of neutrophil elastase (NE) (9), a key cause of elastin fragmentation. Several studies (10) have shown that bacterial neuraminidase influences glucose homeostasis by modulation of sialic acid levels in adipocyte culture. Because binding of EDPs to the ERC is known to trigger sialidase activity (7), we hypothesized that the generation of elastin fragments could modulate IRES development by the chronic involvement of ERC signaling. Using in vivo models, we show here that the chronic presence of EDPs inhibits glucose tolerance, favors lipid accumulation in liver and adipocytes, and promotes IRES.

RESEARCH DESIGN AND METHODS

Animals. Experiments were supervised by one of the authors (S.B.) in agreement with the European legislation on care and use of laboratory animals. C57Bl/6J male mice, aged 8 weeks, were maintained under standard laboratory conditions and then killed by cervical dislocation. Tissues were immediately frozen in liquid nitrogen.

EDPs. KOH hydrolysis was used to prepare κ-elastin (kE), as described previously (11). The synthetic elastin (VGVAPG) and scramble (VVGPGA) peptides were purchased from GeneCust (Dudelange, Luxembourg). kE (1–100 mg/kg), VGVAPG (5–100 mg/kg), or VVGPGA (50 and 100 mg/kg) was injected in the tail vein of the mice. The ERC inhibitors, 2-deoxy-2,3-dehydro-*N*-acetylneuraminic acid (DANA) and chondroitin sulfate (CS), were injected intraperitoneally at 10 g/L (12,13) and 50 mg/kg of body weight (14), respectively.

Metabolic studies. Glucose tolerance and insulin sensitivity tests were performed as reported by Heikkinen et al. (15) on mice fasted for 4 h. Serum glucose, insulin, and triglyceride levels were analyzed as described previously (16). Plasma insulin concentrations were measured by ELISA (Crystal Chem Inc., Downers Grove, IL). Nonesterified fatty acids, triglycerides, total cholesterol, LDL, and HDL were determined by enzymatic assays (Boehringer Ingelheim, Mannheim, Germany). Extracted with trichloroacetate (4%, w/v), hepatic glycogen was quantified by spectrometry. Energy expenditure was measured by indirect calorimetry, using a method adapted from Gao et al. (17) and by body temperature of mice placed at +4°C for 3 h.

RNA preparation and quantitative RT-PCR. RNA were isolated as described previously (18) and converted to cDNA using SuperScript II RT

From [1]Formations de Recherche en Evolution CNRS 3481, Matrice Extracellulaire et Dynamique Cellulaire, Université de Reims Champagne Ardenne, UFR Sciences Exactes et Naturelles, Reims, France; the [2]Institute of Pharmacy, Martin Luther University Halle-Wittenberg, Halle (Saale), Germany; [3]Département de Biopathologie, Institut Jean-Godinot, Centre Régional de Lutte Contre le Cancer, Reims, France; and [4]Pôle Thoracique et Cardio-Vasculaire, Hôpital Robert-Debré, Centre Hospitalier Universitaire de Reims, Reims, France.

Corresponding author: Sébastien Blaise, sebastien.blaise@univ-reims.fr.

Received 29 March 2013 and accepted 1 August 2013.

DOI: 10.2337/db13-0508

This article contains Supplementary Data online at http://diabetes.diabetesjournals.org/lookup/suppl/doi:10.2337/db13-0508/-/DC1.

S.B., B.R., and C.K. contributed equally to this work.

(Invitrogen Life Technologies) and oligo dT24 primers. Quantitative RT-PCR was performed using the SYBR Green JumpStart PCR kit (Sigma-Aldrich, St. Louis, MO) according to the supplier's protocol. 36B4 and 18S RNAs were used as internal controls.

Histology and immunohistology. Cryosections (4 μm) from liver or adipose tissue samples were stained with hematoxylin-eosin or Oil-Red-O, as described previously (19). Lipid droplet areas were counted in six sections using ImageJ software. For immunohistology, cryosections were incubated overnight at 4°C with primary antibodies (Supplementary Table 1). After further incubation for 1 h with an Alexa Fluor-conjugated secondary antibody (1:1000; Molecular Probes) in PBS containing 10% bovine serum, samples were visualized by confocal microscopy.

Immunoprecipitation and Western blotting. Tissue or 3T3-L1 cells were prepared as described previously (20). In brief, 500 μg protein lysate was immunoprecipitated using 1 μg anti–insulin receptor (IR) or anti–Neu-1 antibody overnight at 4°C, followed by 20% protein G-Sepharose (100 μL; Amersham Pharmacia Biotech) for 5 h. Denatured in loading buffer, the resulting proteins were used for immunoblotting. Analyses were performed with primary antibodies using 40 μg tissue or cell extract (20). To visualize the sialylated glycoprotein bands from immunoprecipitated β-subunits of IR, the membranes were then probed with the Dig-MAA (Roche Digoxigenin Glycan Differentiation kit), recognizing α2-3–linked sialic acids, in accordance with the manufacturer's protocol. Bands were quantitated by densitometry using ImageJ software.

Modeling analysis

Homology modeling. A homology model of human Neu-1 was built using MODELLER software (5) and the crystallographic data available for *Micromonospora viridifaciens* sialidase (PDB entry 1EUR). The resulting 100 models produced were ranked according to their objective function values and the best one was conserved for the docking experiments.

Docking. Docking of the sialic acid on the IR was performed using the AutoDock 4.0 software (7). Protein/protein docking experiments were performed using the Rosetta (8) software.

Statistical analyses. Results were expressed as means ± SD. Student's *t*-test and Mann-Whitney *U*-tests were used when appropriate. For all analyses, at least three independent experiments (each including at least five mice) were performed. Values of $P < 0.05$ were considered significant.

RESULTS

Quality and composition of the kE preparations. Although kE has been widely used for several decades as a substrate to mimic elastin degradation products, virtually nothing is known about its exact composition. Hence, three batches of kE preparations were analyzed by liquid chromatography and tandem mass spectrometry (LC/MS/MS). The lengths of the identified kE peptides were between 9 and 23 amino residues and originated from different regions of elastin's precursor. We further found that *1*) the kE preparations were qualitatively highly consistent and that *2*) most of the detectable peptides were assigned to bovine elastin (Supplementary Table 1) and only very few peptides (<5%) were matched to bovine collagens.

EDPs trigger transient hyperglycemia in mice. To determine if EDPs have an effect on glucose homeostasis, we performed a single intravenous injection of kE in fasted mice. Blood glucose levels were measured after 30 min. A significant increase of glycemia was observed after a single injection of kE (10 mg/kg) (Fig. 1*A*). Higher doses also increased glycemia but failed to promote a stronger effect. The canonical EDP VGVAPG induced an effect similar to kE but at higher concentrations, whereas the VVGPGA scramble had no observable effect on glycemia. The greatest efficacy of kE in increasing glycemia was also confirmed by comparing the effects of injection of 10 mg/kg kE (Supplementary Fig. 1*A*), 50 mg/kg VGVAPG (Supplementary Fig. 1*B*), or 100 mg/kg VVGPGA (Supplementary Fig. 1*C*). Although the scramble peptide had no effect, synthetic VGVAPG increased blood glucose to 40% basal levels after 1 h, whereas the same effect was observed for kE after 30 min. To confirm this hyperglycemic effect, a bolus of increasing concentrations of kE was intravenously injected into a second batch of fasted mice every 30 min, and blood glucose levels were measured (Supplementary Fig. 1*D*). Compared with vehicle (PBS injection), a significant increase in glycemia was observed at each time point after injection of kE at 10 mg/kg. Higher doses also increased glycemia but did not promote a stronger effect. At the end of the experiment, kE had induced a 38% increase in blood glucose ($P = 0.0283$), confirming its hyperglycemic effect. Taken together, our data demonstrate that kE increased glycemia in vivo. Furthermore, this effect could be due to a variety of bioactive xGxxPG sequences (sequences known to bind the ERC) present in kE. MS investigations of kE showed that it contains, for instance, peptides with the bioactive motifs PGAIPG, GAVPG, GVLPG, GGVPG, and GVVPG (Supplementary Table 2). The variety of these motifs could explain the stronger effect of kE compared with VGVAPG.

Because kE had a stronger effect than VGVAPG at the same concentration, kE at 10 mg/kg was used in the subsequent experiments.

To determine how EDPs exert their effect, ex vivo effects of kE on soleus muscle glucose uptake were analyzed in the presence or absence of insulin (Fig. 1*B*). Under both conditions, kE limited glucose uptake by soleus muscle in a dose-dependent manner, with a significant effect at 50 mg/mL, suggesting that the effect was independent of insulin. Similar effects were also observed in liver (Supplementary Fig. 1*E*) and perigonadal white adipose tissue (WAT) (Supplementary Fig. 1*F*). These results led us to incubate the tissues with insulin in the subsequent glucose uptake tests and ex vivo experiments. Because the effects of EDP treatment on blood glucose homeostasis appeared to be independent of insulin presence, we hypothesized that they could be due to reduced glucose transport in tissues.

Chronic accumulation of EDPs promotes glucose intolerance in mice. In diabetic mice, we observed a high fragmentation of aortic elastin (Supplementary Fig. 2*A*) and an increase of EDP blood concentrations (Supplementary Fig. 2*B*). The EDP concentration to inject was selected based on the above results, the administration mode (bolus), and the observed elimination conditions. With intravenous injection of kE at 10 mg/kg (Supplementary Fig. 2*C*), only half of the injected EDPs remained in plasma after 10 min. One day after injection, less than 10% was detected, the remainder having been incorporated in tissue or eliminated in urine. One hour after injection, 50% of the injected kE was measured in urine and almost 100% at 1 day (Supplementary Fig. 2*D*). These results suggest that EDPs are rapidly eliminated in vivo. Therefore, weekly intravenous injections of a high concentration of kE (10 mg/kg) were performed for 2 months to evaluate the effects of long-term exposure in vivo.

Injections of kE induced significant hyperglycemia in fed mice as early as the fifth week (Fig. 1*C*). Glycemia returned to basal levels when kE treatment was stopped. Strikingly, renewed injection of kE resulted in rapid hyperglycemia. We also verified that repeated injections of kE did not induce IgG against EDPs (i.e., kE was not immunogenic and did not respond to glucose dysregulation; data not shown). Similarly, food intake did not significantly increase during kE treatment (Fig. 1*D*). Moreover, the body weight of these mice increased after kE injections and was sustained even when kE treatment was stopped (Fig. 1*E*). These results suggest that hyperglycemia is kE-dependent and body weight–independent.

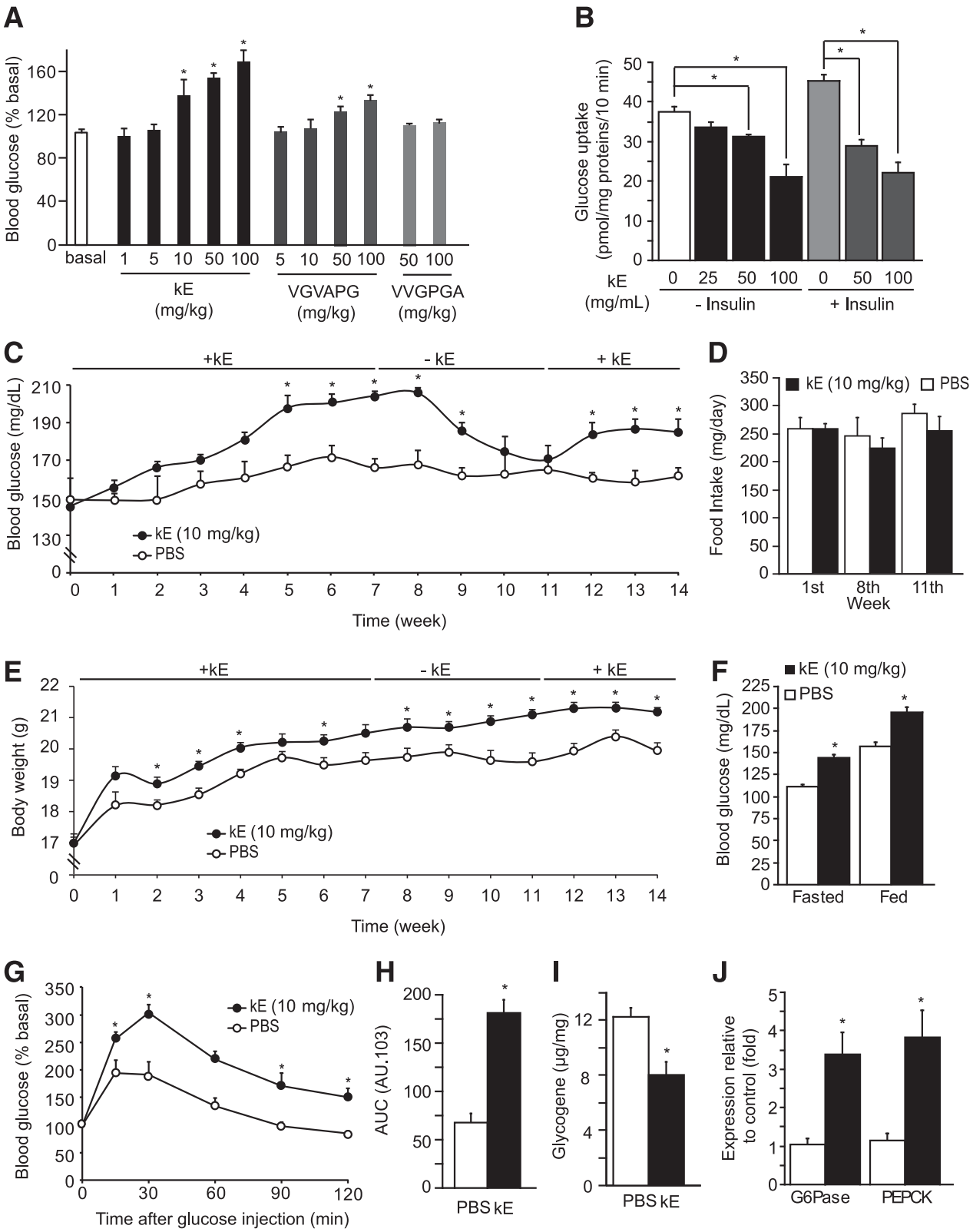

FIG. 1. Hyperglycemia is increased by EDP injections. *A:* **Blood glycemia 30 min after an intravenous single injection of various doses of kE, VGVAPG, or VVGPGA (n = 7).** *B*: **Glucose uptake measured in isolated soleus muscles incubated with kE with (dark gray bars) or without insulin (black bars). White and light gray bars correspond to conditions without kE insulin at the indicated concentrations (n = 5 per group).** *C*: **Time-course study of blood glucose after intravenous injection of kE once weekly compared with fed mice injected with PBS (n = 10 per group).** *D*: **Food intake obtained at 1, 8, and 11 weeks (n = 5 per group).** *E*: **Time-course study of blood glucose after intravenous injection of kE once weekly (n = 5 per group).** *F*: **Blood glucose level in mice fasted 6 h and treated for 7 weeks with kE or PBS (n = 9 per group).** *G*: **Results of glucose tolerance test (GTT) at the seventh week of injections in mice after 6-h fast (n = 10 per group).** *H*: **The bar graph represents the average area under the curve (AUC) of the GTT results.** *I*: **Glycogen quantification in mice fasted 6 h and treated for 7 weeks with kE or PBS (n = 5 per group).** *J*: **Glucose 6 phosphatase (G6Pase) and phosphoenolpyruvate carboxykinase (PEPCK) expressions by quantitative real-time PCR, in liver of fasted mice treated or not with kE for 7 weeks. Target mRNA levels were normalized to 36B4 mRNA levels (n = 6–9). Results are the mean ± SEM. Statistically significant differences (*P < 0.05, Mann-Whitney).**

To confirm the hyperglycemic effect of chronic EDP exposure, mice were treated weekly with kE (10 mg/kg), and glucose tests were performed on the fifth day after injections. At the seventh week after injection, the body weight of mice treated with PBS and kE was 19.7 ± 0.2 g and 20.5 ± 0.2 g, respectively ($P = 0.0783$). Glycemia was assessed in fed and fasted mice (Fig. 1*F*). Because fasted mice were found to be hyperglycemic, we concluded that hyperglycemia was induced by EDP treatment. Analysis of the area under the curve of glucose tolerance tests after intraperitoneal injection of glucose or PBS (Fig. 1*G*) revealed that glucose tolerance was markedly impaired in treated compared with control mice (Fig. 1*H*). Interestingly, the hyperglycemia observed during kE treatment was associated with decreased glycogen storage (Fig. 1*I*) and increased glucose-6-phosphatase and phosphoenolpyruvate carboxykinase mRNA expression (Fig. 1*J*), suggesting activation of glycogenolysis and gluconeogenesis.

In summary, mice that experienced chronic accumulation of EDPs developed some characteristic features of IRES syndrome, including hyperglycemia, glucose intolerance, and gluconeogenesis activation.

EDPs alter energetic metabolism in mice. We previously showed a body weight gain in mice injected with EDPs compared with control mice (Fig. 1*E*). These metabolic changes between control and treated mice were caused by a decrease of O_2 consumption (Fig. 2*A*), an increase in the respiratory quotient (Fig. 2*B*), and a decrease of total energy expenditure (Fig. 2*C*). We also showed that the change in total energy expenditure correlated with alteration of mRNA expression involved in thermoregulation homeostasis (Supplementary Fig. 3*A* and *B*). The observed decrease of energy expenditure suggests that fat mobilization was decreased in mice treated with EDPs. Strikingly, EDP treatment was associated with significantly higher plasma levels of LDL, free fatty acids, and triglycerides (Table 1) in fasted mice. Lipid metabolism dysregulation was further confirmed by an increase of fat pad weight (Supplementary Fig. 3*C*), BMI (Supplementary Fig. 3*D*), and waist circumference (Supplementary Fig. 3*E*) in mice injected with kE compared with control mice.

In liver, histological analysis (Fig. 2*D*) and Oil-Red-O staining quantification (Fig. 2*E*) showed that mice injected with kE accumulated lipid droplets. Accordingly, expression of acetyl CoA carboxylase (ACC) and fatty acid synthase (FAS) was increased in liver after treatment with kE (Fig. 2*F*). As previously described, we observed a decrease of peroxisome proliferator–activated receptor-γ coactivator 1-α (PGC1-α) and peroxisome proliferator–activated receptor-α (PPAR-α) mRNA expression in skeletal muscle (Supplementary Fig. 3*F*).

Hypertrophy of perigonadal WAT was evidenced by histological analysis (Fig. 2*G*) and the quantification of cell areas (Fig. 2*H*). Adipocyte remodeling may be explained by increased PPARγ and C/EBPα mRNA expression (Fig. 2*I*). Expression of PPARγ target genes, ACC and FAS, was also highly increased. These results suggest that lipogenesis was affected by kE injections. The histological analysis (Fig. 2*J*) showed slight increases in CD68, a marker of macrophages, and in myeloperoxidase, a marker of neutrophil granulocytes.

Finally, to confirm these results, mature adipocytes obtained by classical differentiation of 3T3-L1 were incubated with different concentrations of kE, VGVAPG, or VVGPGA. Oil-Red-O accumulation in cells was proportional to kE or VGVAPG concentrations (Supplementary Fig. 3*G* and *H*), in contrast to the scramble peptide. As previously described (21–23), we showed that kE (50 μg/mL) and VGVAPG (200 μg/mL) were the optimal concentrations needed to induce biological effects in vitro. In parallel, mRNA levels of PPARγ and C/EBPα were significantly increased (Supplementary Fig. 3*I*), confirming that kE induces in vitro lipogenesis in adipocytes.

EDP-treated mice exhibit decreased insulin sensitivity. Because the observed hyperglycemia and lipid accumulation in mice suggested that EDP treatment induced insulin pathway alteration (24), we analyzed insulin synthesis and secretion. Under basal conditions, no difference was observed in pancreas mass (Supplementary Fig. 4*A*) and Langerhans islet area (Supplementary Fig. 4*B* and *C*). In agreement with the observed hyperinsulinemia (Fig. 3*A*), immunohistochemistry experiments (Supplementary Fig. 4*B* and *D*) showed that kE decreased glucagon synthesis and increased insulin synthesis. Moreover, insulin synthesis and secretion after glucose stimulation were not significantly modified in mice treated with kE compared with control mice (Supplementary Fig. 4*E* and *F*). These results suggest that EDPs do not affect insulin secretion by β-cells. To determine whether the observed hyperglycemia was due to IRES, homeostasis model assessment (HOMA) of IRES (15) was calculated (Fig. 3*B*). Increased values of HOMA-IRES in treated mice confirmed that kE induces IRES. Insulin-stimulated glucose uptake tests revealed that kE affects insulin sensibility (Fig. 3*C* and *D*). Analysis of the insulin pathway showed that kE decreases IR phosphorylation on Y-972 in skeletal muscle (Fig. 3*E*/H), suggesting inhibition of IR activity and the corresponding signaling pathway (25,26). In addition, decreased phosphorylation of Akt and forkhead box proteins O1 (Foxo-1 was observed. This reduction of phosphorylation was accompanied by increased expression of gluconeogenesis enzymes (Fig. 1*J*). Similar effects were also observed in liver (Fig. 3*F* and *I*) and WAT (Fig. 3*G* and *J*).

These results suggest that EDPs may decrease the insulin pathway by reducing IR activity in tissues involved in glucose homeostasis regulation.

ERC reduces IR signaling. Binding of EDP to the ERC induces various signaling pathways (7). To determine if ERC-related signaling could influence IR activity, we used intraperitoneal injections of DANA, an inhibitor of Neu-1 catalytic activity, and CS, a known antagonist of EDP binding onto EBP. Glycemia in mice treated with kE returned to basal levels 30 min after intraperitoneal injections of DANA and CS (Fig. 4*A*). Although no difference was observed in mice injected with PBS (Fig. 4*B* and *D*), insulin tolerance tests showed that in mice injected with kE, insulin sensitivity was significantly increased in the presence of DANA and CS (Fig. 4*C* and *D*). Ex vivo, we observed that these inhibitors restored glucose uptake (Fig. 5*A*), IR phosphorylation (Fig. 5*D*), and Foxo-1 phosphorylation (Fig. 5*G*) in soleus muscle. Similar effects were also observed in liver (Fig. 5*B*, *E*, and H) and WAT (Fig. 5*C*, *F*, and *H*). Interestingly, DANA and CS had no effect on glucose metabolism in diabetic mice (Supplementary Fig. 5*A*–*H*). To validate the glucose-uptake restoration by ERC inhibitors, the same experiments were performed in vitro on mature 3T3-L1 adipocytes. With DANA or CS, levels of glucose uptake (Supplementary Fig. 5*I*) and phosphorylation of IR (Supplementary Fig. 5*J*) were similar to the levels in control cells, suggesting that EDPs inhibit IR signaling after their binding to the ERC.

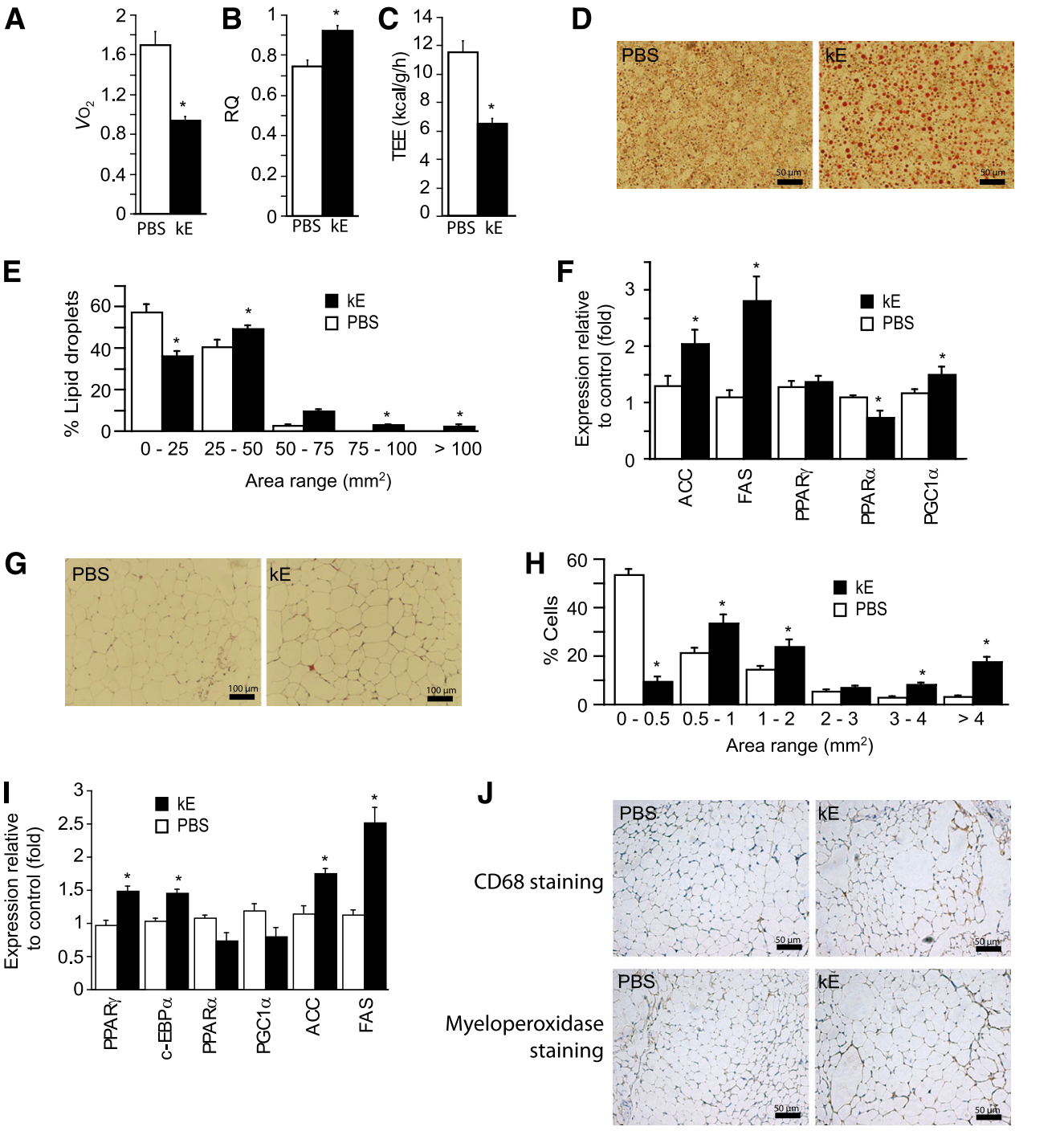

FIG. 2. Decreased energy metabolism effects are shown after 7 weeks of intravenous injections of kE (10 mg/kg) in mice compared with PBS injection for Vo_2 (*A*), the respiratory quotient (RQ) (*B*), and total energy expenditure (TEE) (*C*). *D*: Oil-red-O staining of liver (n = 4). *E*: Quantification of the size of adipocytes observed in *D*. *F*: Expression of hepatic markers of lipogenesis (n = 8). *G*: Hematoxylin-eosin staining of adipose tissue (n = 4). *H*: Quantification of the size of lipid droplets observed in *F*. *I*: Expression of adipose markers of lipogenesis marker in fat (n = 6). *J*: Immunostaining against CD68 and myeloperoxidase on WAT. Results are the mean ± SEM. Statistically significant differences (*P < 0.05, Mann-Whitney).

Mice or cell culture that experienced chronic accumulation of EDPs showed altered IR activity after ERC induction.

Neu-1 interacts with IR and inhibits the insulin-signaling pathway. To further understand the mechanism(s) linking ERC and IR activities, we performed confocal microscopy to analyze Neu-1 and IR in skeletal muscle of mice treated with or without kE (Fig. 6*A*). In the absence of kE, IR was localized at the membrane and Neu-1 was barely expressed and localized at the membrane. In contrast, when cells were treated with kE, Neu-1 was recruited more into the membrane and colocalized with IR. This suggests that EDPs favor membrane relocalization of Neu-1 and potentiate the interaction between ERC and IR. To confirm this interaction, we performed coimmunoprecipitations from isolate skeletal muscles (Fig. 6*B* and *C*). In the absence of kE stimulation, few interactions were observed between the two receptors.

TABLE 1
Plasma lipid analysis

	PBS	kE	*P*
Cholesterol (mmol/L)			
Total	1.68 ± 0.17	1.68 ± 0.31	0.7728
HDL	1.24 ± 0.15	1.15 ± 0.35	0.7865
LDL	**0.43 ± 0.04**	**0.54 ± 0.01**	**0.0366**
Free fat acids (mEq/L)	**0.33 ± 0.02**	**0.65 ± 0.11**	**0.0017**
Triglycerides (mmol/L)	**0.40 ± 0.01**	**0.51 ± 0.03**	**0.0146**

Results are the mean ± SEM (n = seven per group). Data in boldface indicate statistically significant differences ($P < 0.05$, Mann-Whitney).

Incubation with kE increased the interaction between Neu-1 and IR. Treatment with DANA had no effect, but CS blocked the coimmunoprecipitation. Similar effects were observed in vitro in mature adipocytes (Supplementary Fig. 5*K*). These in vivo and in vitro results demonstrate that Neu-1 and IR interact together upon EDP stimulation.

Interaction between these receptors was analyzed by molecular and docking modeling between Neu-1 and the extracellular part of the IR (Fig. 6*D*). This analysis highlighted that Neu-1 interacts directly with the IR β-chain in a region rich in sialic acid without hampering the interaction between insulin and the α-chain of the receptor. The level of sialic acid has been described as a regulator of IR and IRES (27). To show whether Neu-1 can modulate the IR sialylation level, IR was immunoprecipitated from skeletal muscle and the level of sialic acid quantified. In vivo (Fig. 6*E*) and ex vivo (Fig. 6*F*), we observed that kE decreased the level of sialic acids of IR of skeletal muscle. In contrast, inhibition of Neu-1 activity by DANA or of kE binding on EBP by CS restored the sialylation of IR. These results were associated with the observed decrease of IR signaling (Fig. 5).

DISCUSSION

Previous clinical or in vivo studies (9,28) have suggested that serum elastase activity and EDP levels are increased

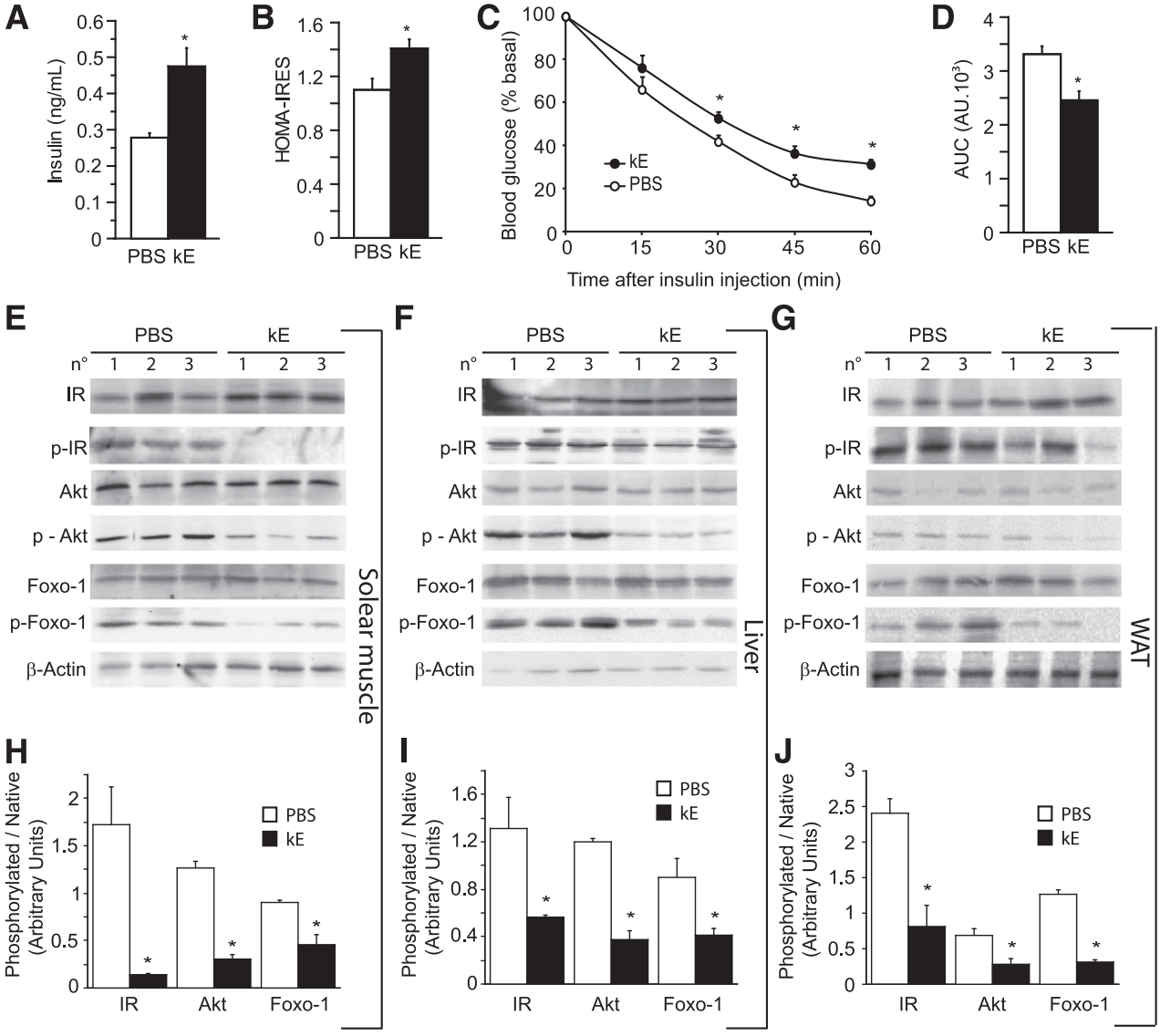

FIG. 3. Increased IRES in mice treated with kE or PBS. *A*: Blood insulin level (n = 8 per group). *B*: HOMA for IRES. *C*: Results of intraperitoneal insulin sensitivity test (n = 10 per group). D: The bar graph represents the average area under the curve (AUC) of intraperitoneal insulin sensitivity test. Western blot analysis of phosphorylation of IR (Y972), Akt (T308), and Foxo-1 (T24) in solear muscle (*E*), liver (*F*), and WAT (*G*). Actin served as a loading control. Quantification of phosphorylation level in solear muscle (*H*), liver (*I*), and WAT (*J*) tissue. Results are the mean ± SEM. Statistically significant differences (*$P < 0.05$, Mann-Whitney).

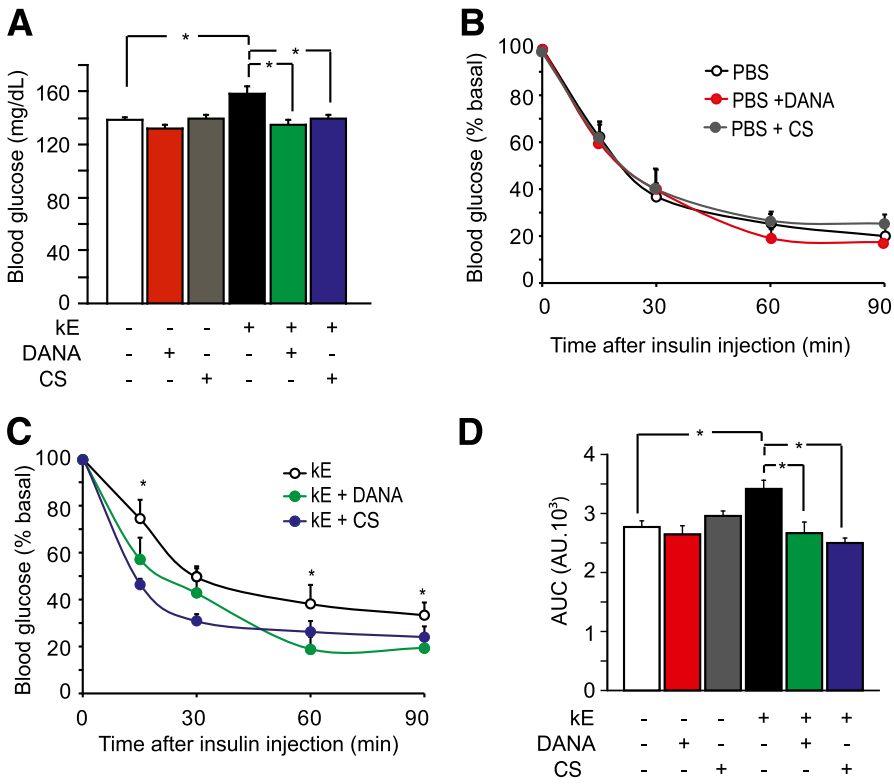

FIG. 4. Restoration of insulin sensitivity by ERC inhibitors in mice treated with kE or PBS. *A*: Blood glucose level measured 30 min after basal condition (without kE, white bar and with kE, black bar), DANA (without kE, red bar and with kE, green bar), and CS injections (without kE, gray bar and with kE, blue bar) ($n = 5$ per group). Intraperitoneal insulin sensitivity test in the presence of DANA or CS in mice treated with PBS (*B*) or kE (*C*) ($n = 5$ per group). *D*: The bar graph represents the average area under the curve (AUC) of the intraperitoneal insulin sensitivity test. Basal condition (without kE, white bar and with kE, black bar), DANA (without kE, red bar and with kE, green bar), and CS injections (without kE, gray bar and with kE, blue bar). Results are the mean ± SEM. Statistically significant differences (*$P < 0.05$, Mann-Whitney).

in obesity and diabetes. According to studies by Robert and colleagues (28–32), the concentration of anti-EDP antibodies of IgG is increased threefold in type 2 diabetic (T2D) patients compared with the control population. Because elastin fragmentation is an earlier event than T2D, we surmised that EDP accumulation might influence glucose homeostasis. The current study shows, for the first time, that EDP accumulation induces IRES without altering insulin secretion. With an EDP concentration (10 mg/kg) inferior to that observed in diabetic mice (15 mg/kg), we showed that a single injection increased glycemia transiently, whereas chronic injections induced stable glucose intolerance.

The observed elastokine-dependent hyperglycemia was explained by an alteration of IR signaling in tissues. Thus, decreased phosphorylation of IR, Akt, and Foxo-1 (26) activated gluconeogenesis (25) and inhibited glucose uptake.

In accordance with several studies (33–35) demonstrating that ECM influences lipid metabolism, we show for the first time that matrikines, such as EDPs, play an important role in adipose tissue and liver remodeling as well as in energy metabolism. EDP treatment induced adipocyte hypertrophy of mice perigonadal WAT (by the activation of PPARγ, ACC, and FAS) and favored the development of hepatic steatosis associated with an increase of PCG-1α (20). In skeletal muscle, decreased PGC-1α expression due to EDP accumulation could favor the development of IRES. Indeed, increased PGC-1α expression has been reported in the liver of T2D mouse models in contrast to decreased expression observed in muscles from human T2D subjects (36,37). EDP accumulation in mice fed with a chow diet induced hyperglycemia together with lipid accumulation, as observed in more than 80% of patients with T2D (38–40).

Recently, Talukdar et al. (9) showed that NE induced IRES in mice fed with a high-fat diet. In vitro, IR could also be affected by Neu-1 sialidase activity in skeletal and smooth muscle cells (41). The underlying mechanisms remain unknown; however, a previous study showed that NE released a variety of elastin peptides containing bioactive motifs upon degradation of human skin elastin (42). Many of these peptides contain bioactive motifs that are also present in kE such as PGAIPG, GLVPG, and GAVPG (Supplementary Table 2). Thus, induction of IRES may be influenced by the liberation of such peptides by NE. From our data, we propose that binding of EDPs and ERC could be involved in the human pathophysiology of IRES. The ERC is expressed at the surface of numerous cell types (43) and is composed of three subunits: EBP (67 kDa) is reported to be peripheral and binds elastin, whereas cathepsin A (61 kDa) and Neu-1 (55 kDa) are membrane-associated. The binding of EDP and EBP can be antagonized by galactosugars, such as lactose or CS (44). Likewise, Neu-1 enzymatic activity can be efficiently inhibited by DANA (8). These inhibitors restored glucose uptake and phosphorylation of IR and Foxo-1, suggesting that IR signaling was returned to normal.

The interaction of Neu-1 with the β-chain of the IR is only possible under exposure to EDPs and is blocked by CS, implying that this interaction is EDP-dependent. Further, as observed for IR signaling and the Neu-1–IR interaction, we demonstrated that kE exposure decreased the sialic acid level on the β-chain of the IR. This effect could be explained by the activation of subunit Neu-1,

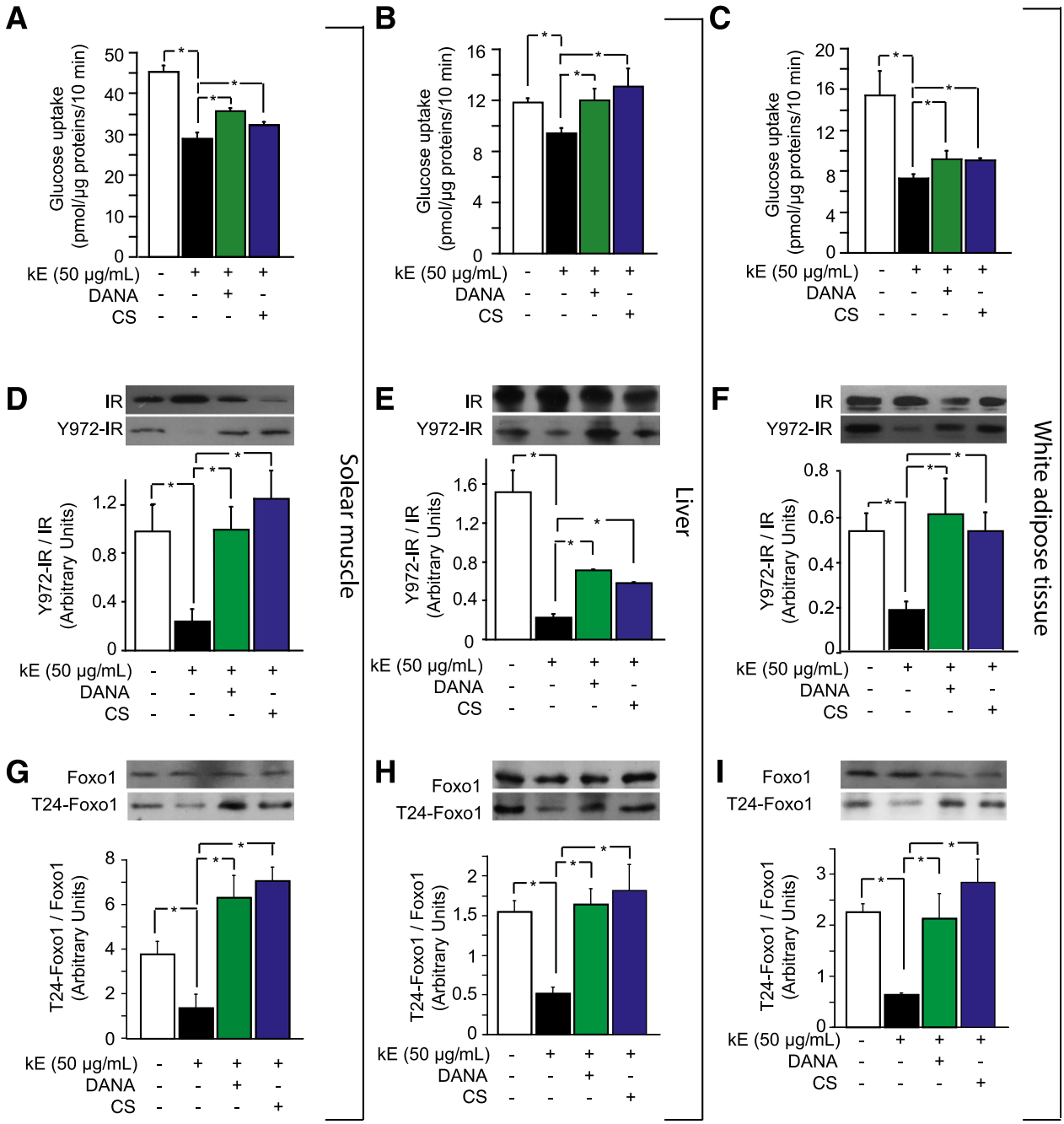

FIG. 5. Restoration ex vivo of insulin signaling by ERC inhibitors. Glucose uptake in isolated solear muscle (*A*), liver (*B*), and WAT (*C*) in presence or not of DANA or CS (n = 5 per group). Quantification of IR phosphorylation (Y972) level in solear muscle (*D*), liver (*E*), and WAT (*F*). Quantification of Foxo-1 phosphorylation (T24) level in solear muscle (*G*), liver (*H*), and WAT (*I*). Results are the mean ± SEM. Statistically significant differences (*$P < 0.05$, Mann-Whitney). Basal condition (white bar), kE incubation (black bar), treatment with DANA (green bar) and with CS (blue bar).

which is a sialic acid hydrolase that specifically clips off terminally located sialic acid on protein surfaces. Our findings support the recent work of Dridi et al. (45), who demonstrated that Neu-1 can interact and desialylate IR. Surprisingly, they showed that the interaction is insulin-dependent and upregulates IR signaling. In contrast, several studies (10,27) have suggested that the decrease of sialic acids on the IR reduces signal transduction from insulin binding to glucose transport and lipolysis. Moreover, Hayes and Lockwood (46) have shown that treatment of cells with bacterial neuraminidase inhibits IR phosphorylation and loss of sialic acids on the IR, resulting in total loss of insulin action. We think that the activity of Neu-1 induced by EDPs could be responsive to the decrease of sialic acids on the IR and reduction in IR signaling. The effects on IR signaling could depend on several factors such as the nature, localization, and number of sialic acids on the IR. No study has yet demonstrated this hypothesis.

In conclusion, our study showed for the first time, in vivo and in vitro, that EDPs were able to induce IRES associated with tissue remodeling. As a consequence, we propose that these matrikines are newly discovered regulators of IR activity. The fragmentation of elastin and formation of EDPs are aging markers and could therefore be

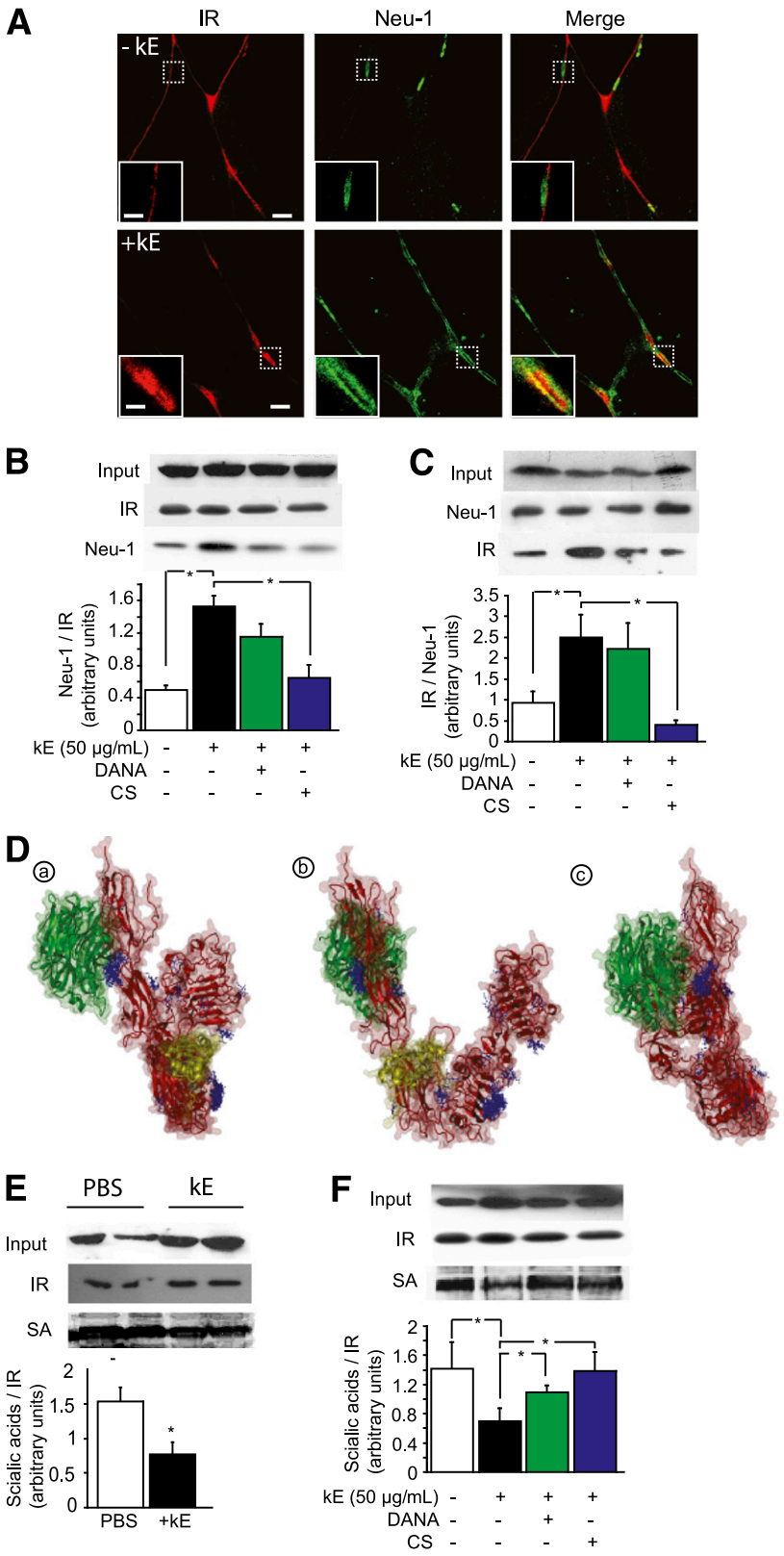

FIG. 6. ERC interplay and desialilate IR in the presence of EDP. *A*: Immunohistofluorescence of IR (red) and Neu-1 (green) in solear muscle analysis by confocal microscopy (n = 3). Bars: 5 µm; inset bar: 2.5 µm. *B*: Immunoprecipitation of IR from skeletal muscle and Western blotting of Neu-1 in presence or not of DANA and CS (*top panel*) and quantification (*bottom panel*) (n = 4). *C*: Immunoprecipitation of Neu-1 from skeletal muscle and Western blotting of IR in presence or not of DANA and CS (*top panel*) and quantification (*bottom panel*) (n = 4). *D*: Direct docking between Neu-1 (green) and extracellular part of β- and α-chains of IR (red) and insulin (yellow). Potential sialic acid sites are in blue. Different views of this docking are shown in *a* to *c*. *E*: Immunoprecipitation of IR in vivo from solear muscle and sialylation level of the receptor (*top panel*) and quantification (*bottom panel*) (n = 4 per group). *F*: Immunoprecipitation of IR and sialilation level from isolated solear muscle incubated or not, ex vivo, with DANA or CS (*top panel*) and quantification (*bottom panel*) (n = 4 per group). Basal condition (white bar), kE incubation (black bar), treatment with DANA (green bar) and with CS (blue bar). Statistically significant differences (*P < 0.05, Mann-Whitney).

considered as insidious mechanisms favoring IRES development. Overall, our results strongly suggest that EDPs could be key factors involved in the onset of T2D, a disease that is more prevalent in aged subjects.

ACKNOWLEDGMENTS

This work was supported by funding from the CNRS and by Université de Reims Champagne Ardenne.

No potential conflicts of interest relevant to this article were reported.

S.Bl. wrote the manuscript and researched data. B.R., C.K., M.G., F.R., C.G., and M.D. researched data. S.Ba., L.Du., and P.M. reviewed the manuscript. A.H. and C.E.H.S. researched data and reviewed the manuscript. M.T and L.M. contributed to discussion. L.De. and V.D. reviewed the manuscript. S.Bl. is the guarantor of this work and, as such, had full access to all the data in the study and takes responsibility for the integrity of the data and the accuracy of the data analysis.

The authors acknowledge the technical assistance of Annie Carlier, Christine Terryn, and the imaging platform Infrastructure en Biologie, Santé et Agronomie (IBISA) (University of Reims Champagne-Ardenne, Reims), as well as the Molecular Modeling Platform and the ROMEO High Performance Computing Center, Reims.

REFERENCES

1. Maurice P, Blaise S, Gayral S, et al. Elastin fragmentation and atherosclerosis progression: The elastokine concept. Trends Cardiovasc Med 2013;23:211–221
2. Mithieux SM, Weiss AS. Elastin. Adv Protein Chem 2005;70:437–461
3. Shapiro SD, Campbell EJ, Welgus HG, Senior RM. Elastin degradation by mononuclear phagocytes. Ann N Y Acad Sci 1991;624:69–80
4. O'Rourke MF. Arterial aging: pathophysiological principles. Vasc Med 2007;12:329–341
5. Fulop T, Khalil A, Larbi A. The role of elastin peptides in modulating the immune response in aging and age-related diseases. Pathol Biol (Paris) 2012;60:28–33
6. Blanchevoye C, Floquet N, Scandolera A, et al. Interaction between the elastin peptide VGVAPG and human elastin binding protein. J Biol Chem 2013;288:1317–1328
7. Duca L, Blanchevoye C, Cantarelli B, et al. The elastin receptor complex transduces signals through the catalytic activity of its Neu-1 subunit. J Biol Chem 2007;282:12484–12491
8. Amith SR, Jayanth P, Franchuk S, et al. Dependence of pathogen molecule-induced toll-like receptor activation and cell function on Neu1 sialidase. Glycoconj J 2009;26:1197–1212
9. Talukdar S, Oh Y, Bandyopadhyay G, et al. Neutrophils mediate insulin resistance in mice fed a high-fat diet through secreted elastase. Nat Med 2012;18:1407–1412
10. Fujita-Yamaguchi Y, Sato Y, Kathuria S. Removal of sialic acids from the purified insulin receptor results in enhanced insulin-binding and kinase activities. Biochem Biophys Res Commun 1985;129:739–745
11. Brassart B, Fuchs P, Huet E, et al. Conformational dependence of collagenase (matrix metalloproteinase-1) up-regulation by elastin peptides in cultured fibroblasts. J Biol Chem 2001;276:5222–5227
12. Calfee DP, Peng AW, Cass LM, Lobo M, Hayden FG. Safety and efficacy of intravenous zanamivir in preventing experimental human influenza A virus infection. Antimicrob Agents Chemother 1999;43:1616–1620
13. Colman PM. A novel approach to antiviral therapy for influenza. J Antimicrob Chemother 1999;44 (Suppl. B):17–22
14. Zhou J, Nagarkatti P, Zhong Y, Nagarkatti M. Immune modulation by chondroitin sulfate and its degraded disaccharide product in the development of an experimental model of multiple sclerosis. J Neuroimmunol 2010;223:55–64
15. Heikkinen S, Argmann CA, Champy MF, Auwerx J. Evaluation of glucose homeostasis. Curr Protoc Mol Biol 2007;Chapter 29:Unit 29B.23
16. Picard F, Géhin M, Annicotte J, et al. SRC-1 and TIF2 control energy balance between white and brown adipose tissues. Cell 2002;111:931–941
17. Gao Q, Mezei G, Nie Y, et al. Anorectic estrogen mimics leptin's effect on the rewiring of melanocortin cells and Stat3 signaling in obese animals. Nat Med 2007;13:89–94
18. Blaise S, Kneib M, Rousseau A, et al. In vivo evidence that TRAF4 is required for central nervous system myelin homeostasis. PLoS ONE 2012;7:e30917
19. Blaise SA, Alberto JM, Audonnet-Blaise S, Guéant JL, Daval JL. Influence of preconditioning-like hypoxia on the liver of developing methyl-deficient rats. Am J Physiol Endocrinol Metab 2007;293:E1492–E1502
20. Pooya S, Blaise S, Moreno Garcia M, et al. Methyl donor deficiency impairs fatty acid oxidation through PGC-1α hypomethylation and decreased ER-α, ERR-α, and HNF-4α in the rat liver. J Hepatol 2012;57:344–351
21. Devy J, Duca L, Cantarelli B, et al. Elastin-derived peptides enhance melanoma growth in vivo by upregulating the activation of Mcol-A (MMP-1) collagenase. Br J Cancer 2010;103:1562–1570
22. Chang CH, Kawa Y, Tsai RK, et al. Melanocyte precursors express elastin binding protein and elastin-derived peptide (VGVAPG) stimulates their melanogenesis and dendrite formation. J Dermatol Sci 2008;51:158–170
23. Ntayi C, Labrousse AL, Debret R, et al. Elastin-derived peptides upregulate matrix metalloproteinase-2-mediated melanoma cell invasion through elastin-binding protein. J Invest Dermatol 2004;122:256–265
24. Samuel VT, Shulman GI. Mechanisms for insulin resistance: common threads and missing links. Cell 2012;148:852–871
25. Gross DN, van den Heuvel AP, Birnbaum MJ. The role of FoxO in the regulation of metabolism. Oncogene 2008;27:2320–2336
26. Kanai F, Ito K, Todaka M, et al. Insulin-stimulated GLUT4 translocation is relevant to the phosphorylation of IRS-1 and the activity of PI3-kinase. Biochem Biophys Res Commun 1993;195:762–768
27. Salhanick AI, Amatruda JM. Role of sialic acid in insulin action and the insulin resistance of diabetes mellitus. Am J Physiol 1988;255:E173–E179
28. Bizbiz L, Robert L. Micro-methods for serial determinations of elastin metabolism parameters in blood plasma and serum. Pathol Biol (Paris) 1996;44:694–700
29. Bako G, Jacob MP, Fulop T Jr, Foris G, Leovey A, Robert L. Immunology of elastin: study of anti-elastin peptide antibodies by DOT immunobinding assay. Immunol Lett 1987;15:187–192
30. Fülöp T Jr, Wei SM, Robert L, Jacob MP. Determination of elastin peptides in normal and arteriosclerotic human sera by ELISA. Clin Physiol Biochem 1990;8:273–282
31. Fulop T Jr, Jacob MP, Robert L. Determination of anti-elastin peptide antibodies in normal and arteriosclerotic human sera by ELISA. J Clin Lab Immunol 1989;30:69–74
32. Bizbiz L, Alpérovitch A, Robert L. Aging of the vascular wall: serum concentration of elastin peptides and elastase inhibitors in relation to cardiovascular risk factors. The EVA study. Atherosclerosis 1997;131:73–78
33. Cristancho AG, Lazar MA. Forming functional fat: a growing understanding of adipocyte differentiation. Nat Rev Mol Cell Biol 2011;12:722–734
34. Yang M, Zhang Y, Pan J, et al. Cathepsin L activity controls adipogenesis and glucose tolerance. Nat Cell Biol 2007;9:970–977
35. Motrescu ER, Blaise S, Etique N, et al. Matrix metalloproteinase-11/stromelysin-3 exhibits collagenolytic function against collagen VI under normal and malignant conditions. Oncogene 2008;27:6347–6355
36. Westerbacka J, Kolak M, Kiviluoto T, et al. Genes involved in fatty acid partitioning and binding, lipolysis, monocyte/macrophage recruitment, and inflammation are overexpressed in the human fatty liver of insulin-resistant subjects. Diabetes 2007;56:2759–2765
37. Coste A, Louet JF, Lagouge M, et al. The genetic ablation of SRC-3 protects against obesity and improves insulin sensitivity by reducing the acetylation of PGC-1alpha. Proc Natl Acad Sci U S A 2008;105:17187–17192
38. Nadler ST, Stoehr JP, Schueler KL, Tanimoto G, Yandell BS, Attie AD. The expression of adipogenic genes is decreased in obesity and diabetes mellitus. Proc Natl Acad Sci U S A 2000;97:11371–11376
39. Smyth S, Heron A. Diabetes and obesity: the twin epidemics. Nat Med 2006;12:75–80
40. Neeland IJ, Turer AT, Ayers CR, et al. Dysfunctional adiposity and the risk of prediabetes and type 2 diabetes in obese adults. JAMA 2012;308:1150–1159
41. Arabkhari M, Bunda S, Wang Y, Wang A, Pshezhetsky AV, Hinek A. Desialylation of insulin receptors and IGF-1 receptors by neuraminidase-1 controls the net proliferative response of L6 myoblasts to insulin. Glycobiology 2010;20:603–616
42. Heinz A, Jung MC, Jahreis G, et al. The action of neutrophil serine proteases on elastin and its precursor. Biochimie 2012;94:192–202
43. Duca L, Floquet N, Alix AJ, Haye B, Debelle L. Elastin as a matrikine. Crit Rev Oncol Hematol 2004;49:235–244
44. Hinek A, Smith AC, Cutiongco EM, Callahan JW, Gripp KW, Weksberg R. Decreased elastin deposition and high proliferation of fibroblasts from Costello syndrome are related to functional deficiency in the 67-kD elastin-binding protein. Am J Hum Genet 2000;66:859–872
45. Dridi L, Seyrantepe V, Fougerat A, et al. Positive regulation of insulin signaling by neuraminidase 1. Diabetes 2013;62:2338–2346
46. Hayes GR, Lockwood DH. The role of cell surface sialic acid in insulin receptor function and insulin action. J Biol Chem 1986;261:2791–2798